Sains Malaysiana 55(3)(2026): 573-587
http://doi.org/10.17576/jsm-2026-5503-17

Efficient Removal of Metronidazole from Water using Pyrolyzed ZnO-Polyethylene Waste Nanocomposites as an Adsorbent

(Penyingkiran Cekap Metronidazol daripada Air menggunakan Sisa Nanokomposit ZnO-Polietilena yang Dipirolisis sebagai Penyerap)

JA'AFAR YUSUF[1,2], SITI NURUL AIN MD. JAMIL[1,3,*], SHAHRUL AINLIAH ALANG AHMAD[1], AHMAD ADLIE SHAMSURI[4] & MOHAMMAD ABDULLAH[5]

[1]*Chemistry Department, Faculty of Science, Universiti Putra Malaysia, 43400 UPM Serdang, Selangor, Malaysia*
[2]*Department of Pure and Applied Chemistry, Science Faculty, Kaduna State University, 2339 Kaduna, Nigeria*
[3]*Centre for Foundation Studies in Science of Universiti Putra Malaysia, 43400 UPM Serdang, Selangor, Malaysia*
[4]*Institute of Tropical Forestry and Technology, Universiti Putra Malaysia, 43400 UPM Serdang, Selangor, Malaysia*
[5]*Universiti Teknologi MARA Cawangan Johor, Kampus Pasir Gudang, Jalan Purnama, Bandar Seri Alam, 81750 Masai, Johor, Malaysia*

Received: 1 October 2025/Accepted: 4 March 2026

ABSTRACT

Metronidazole (MNZ) is a widely used antibiotic that frequently contaminates aquatic environments, posing risks of antibiotic resistance and toxicity to ecosystems and human health. In this study, zinc oxide–modified polyethylene waste nanocomposites (ZnO-MPEW-NCs) were synthesized using polyethylene waste (PEW) as a matrix and modified with zinc oxide (ZnO) and concentrated sulfuric acid (H_2SO_4). The composites were thermally treated at 300, 400, and 500 °C to produce P300-, P400-, and P500-ZnO-MPEW-NCs. Comprehensive characterization using Fourier-transform infrared spectroscopy (FTIR), field-emission scanning electron microscopy (FESEM), and Brunauer–Emmett–Teller (BET) surface area analysis confirmed successful structural modification, chemical stability, and compositional integrity. Pyrolysis at 500 °C significantly enhanced the textural properties, increasing the specific surface area from 10 to 106 m^2/g. Batch adsorption experiments demonstrated rapid MNZ removal, with equilibrium achieved within 30 min. The P500-ZnO-MPEW-NCs exhibited the highest adsorption capacity (133.75 mg/g) and removal efficiency (99.4%). Kinetic analysis showed that the adsorption process followed the pseudo-second-order model ($R^2 = 0.99941$, $q_{cal} = 9.88$ mg/g), while intraparticle diffusion analysis indicated contributions from both surface adsorption and pore diffusion. Equilibrium data were best described by the Freundlich isotherm ($R^2 = 0.99958$), suggesting multilayer adsorption on a heterogeneous surface dominated by physisorption. Thermodynamic analysis confirmed that adsorption was spontaneous and exothermic, with Gibbs free energy changes ($\Delta G° = -2.90$ to -10.44 kJ/mol), enthalpy changes ($\Delta H° = -10.50$ to -42.88 kJ/mol), and entropy changes ($\Delta S° = -25.5$ to -102 J/(mol.K)). These results demonstrate the strong potential of P500-ZnO-MPEW-NCs as sustainable adsorbents for pharmaceutical removal from water.

Keywords: Adsorption; adsorption isotherms; kinetic model; metronidazole; polyethylene waste; zinc oxide composite

ABSTRACT

Metronidazol (MNZ) ialah antibiotik yang digunakan secara meluas yang kerap mencemari persekitaran akuatik, menimbulkan risiko rintangan antibiotik dan ketoksikan kepada ekosistem dan kesihatan manusia. Dalam kajian ini, nanokomposit sisa polietilena yang diubah suai oleh zink oksida (ZnO-MPEW-NC) telah disintesis menggunakan sisa polietilena (PEW) sebagai matriks dan diubah suai dengan zink oksida (ZnO) dan asid sulfurik pekat (H_2SO_4). Komposit tersebut dirawat secara terma pada suhu 300, 400 dan 500 °C untuk menghasilkan P300-, P400- dan P500-ZnO-MPEW-NC. Pencirian komprehensif menggunakan spektroskopi inframerah transformasi Fourier (FTIR), mikroskopi elektron pengimbasan pancaran medan (FESEM) dan analisis luas permukaan Brunauer–Emmett–Teller (BET) mengesahkan pengubahsuaian struktur, kestabilan kimia dan integriti komposisi yang berjaya. Pirolisis pada suhu 500 °C meningkatkan sifat tekstur dengan ketara, meningkatkan luas permukaan khusus dari 10 hingga 106 m^2/g. Uji kaji penjerapan kelompok menunjukkan penyingkiran MNZ yang cepat dengan keseimbangan dicapai dalam masa 30 minit. P500-ZnO-MPEW-NC menunjukkan kapasiti penjerapan tertinggi (133.75 mg/g) dan kecekapan penyingkiran (99.4%). Analisis kinetik menunjukkan bahawa proses penjerapan mengikuti model pseudo-tertib kedua ($R^2 = 0.99941$, qcal = 9.88 mg/g), manakala analisis resapan intrazarah menunjukkan sumbangan daripada kedua-dua penjerapan permukaan dan resapan liang. Data keseimbangan paling baik diterangkan oleh isoterma Freundlich ($R^2 = 0.99958$), menunjukkan penjerapan berbilang lapisan pada permukaan heterogen yang didominasi oleh fisisorpsi. Analisis termodinamik mengesahkan bahawa penjerapan

adalah spontan dan eksotermik, dengan perubahan tenaga bebas Gibbs ($\Delta G° = -2.90$ hingga -10.44 kJ/mol), perubahan entalpi ($\Delta H° = -10.50$ hingga -42.88 kJ/mol) dan perubahan entropi ($\Delta S° = -25.5$ hingga -102 J/(mol.K)). Keputusan ini menunjukkan potensi kuat P500-ZnO-MPEW-NC sebagai penjerap lestari untuk penyingkiran farmaseutikal daripada air.

Kata kunci: Isoterma penjerapan; komposit zink oksida; metronidazol; model kinetik; penjerapan; sisa polietilena

INTRODUCTION

The advent of antibiotics marks a significant milestone in modern medicine and microbiology, substantially improving the treatment of infectious diseases worldwide (Qin et al. 2021). Despite their life-saving capabilities, global antibiotic consumption has risen sharply in recent years, reaching approximately 40.1 billion defined daily doses in 2018 alone, highlighting growing dependence and potential misuse (Browne et al. 2021). The extensive application of these compounds in human healthcare and agriculture has led to their persistent discharge into aquatic ecosystems, posing serious threats to environmental and public health (Ling et al. 2024; Liu et al. 2024; Pratap et al. 2023; Wang et al. 2024).

Among the many antibiotics detected in the environment, metronidazole (MNZ), a member of the nitroimidazole class, is of particular concern. MNZ is widely employed for the treatment of anaerobic bacterial and protozoal infections in humans and is also used in veterinary medicine, aquaculture, and livestock industries as a therapeutic agent and feed additive (Habibi, Habibi-Yangjeh & Khataee 2023). Although MNZ is partially metabolized in biological systems, its high aqueous solubility (9,500 mg/L) and low biodegradability limit its complete removal during conventional wastewater treatment, resulting in its persistence in natural water bodies (Arienzo & Donadio 2023). Concentrations of MNZ ranging from a few to several nanograms per liter have been detected in surface water, groundwater, and even drinking water sources (Jamshidi et al. 2025). Due to its potential mutagenic and carcinogenic effects, the presence of MNZ, even at trace levels, can disrupt aquatic ecosystems, promote microbial resistance, and pose risks to human health (Es'hagi et al. 2024; Mazloomi et al. 2023).

To mitigate the environmental impact of MNZ and other antibiotics, several conventional treatment technologies have been explored, including ion exchange, membrane filtration, advanced oxidation processes (photo-Fenton), flocculation, adsorption, heterogeneous photocatalysis, ozonation, and reduction using zero-valent iron nanoparticles (Alamgir et al. 2020; Bashiri et al. 2020). Among these, adsorption has emerged as a promising technique due to its operational simplicity, cost-effectiveness, high removal efficiency, and minimal generation of secondary pollutants.

The global plastics market was valued at approximately USD 651.15 billion in 2024 and is projected to grow from USD 678.56 billion in 2025 to nearly USD 980.86 billion by 2034, corresponding to a compound annual growth rate of 4.18% between 2025 and 2034. This growth is driven by increasing demand across multiple sectors, including packaging, automotive, construction, and electronics, as well as a growing emphasis on sustainable and recyclable materials (Lee et al. 2025). However, the rapid expansion of plastic production has resulted in substantial accumulation of polymeric wastes, particularly polyethylene waste (PEW) from industrial applications and consumer products (Hazan et al. 2021). These wastes are often classified as scheduled wastes and are frequently disposed of via incineration, a practice associated with environmental hazards and secondary pollution (Hirata, Kondo & Ozawa 2014).

In this study, zinc oxide (ZnO)–modified polyethylene waste nanocomposites (ZnO–MPEW-NCs) were developed as sustainable adsorbents for the efficient removal of MNZ from aqueous solutions. MNZ is an emerging pharmaceutical contaminant that has received limited attention in previous studies involving ZnO-based composite materials. The nanocomposites were synthesized via a co-precipitation method, followed by chemical integration of ZnO into a sulfuric acid (H_2SO_4)–modified PEW matrix and controlled pyrolysis at different temperatures to enhance crystallinity, surface area, and functional group distribution. Unlike previous studies that focused on rubber waste derived from hand gloves (Muhammad, Abdul Halim & Mohamed Ibrahim 2022) or magnetic tyre-activated carbon–chitosan composites (Mashile et al. 2020), which exhibited comparatively lower adsorption capacities for antibiotics, this work specifically targets a pharmaceutical contaminant and systematically examines the combined effects of ZnO incorporation and thermally transformed PEW structure on adsorption performance. Material characterization was conducted using Fourier-transform infrared spectroscopy (FTIR), field-emission scanning electron microscopy (FESEM), and Brunauer–Emmett–Teller (BET) surface area analysis. Furthermore, adsorption kinetics, isotherms, and thermodynamic parameters were evaluated to elucidate the mechanisms governing MNZ uptake and assess the long-term applicability of ZnO–MPEW-NCs in water treatment systems. Pyrolysis was limited to 500 °C to prevent excessive decomposition of PEW, which could otherwise reduce carbon yield and compromise adsorption capacity.

MATERIALS AND METHODS

PREPARATION OF THE PEW

The PEW used in this study was obtained from the rubber manufacturing industry in Selangor, Malaysia. ZnO was sourced from Merck, Germany. Methanol (99.9% purity),

MNZ, and Sodium hydroxide (99% purity) were provided by R&M Chemicals in Selangor, Malaysia. Hydrochloric acid (HCl) with a purity of 38% and H_2SO_4 at 98% purity were obtained from J.T. Baker in Thailand. All chemicals were utilized as received, without any further purification.

MODIFICATION OF PEW

The PEW was prepared by crushing the polymer into smaller pieces and then grinding it in a grinding machine into powder, which was sieved using a 100 mesh screen. The powder was allowed to settle at room temperature after being dried for 5 h at 50 °C in an oven to eliminate moisture and volatile materials. The PEW was soaked in 50 mL of the solvent (methanol) and dried in an oven overnight at 50 °C to remove any organic residues from the surface of the solid. 15 g of the PEW was dissolved in 30 mL of H_2SO_4 for 1 h. After filtering and thoroughly rinsing with distilled water, the modified polyethylene waste (MPEW) was allowed to soak for 1 h in 40 mL of 20% (w/v) NaOH. The MPEW was dried in an oven at 75 °C for 12 h after being cleaned with distilled water until it reached a neutral pH.

SYNTHESIS OF ZnO-MPEW-NCs

ZnO-MPEW-NCs were prepared using the co-precipitation method. 5 g of ZnO and 5g of PEW were mixed in a 250 mL conical flask with 100 mL of distilled water. The precipitate formed was filtered, washed with distilled water several times, and dried at room temperature. The resulting composite was referred to as ZnO-MPEW-NCs. The composites were then pyrolyzed at 300 °C, 400 °C, and 500 °C with a heating rate of 10 °C/min for 1 h under constant nitrogen flow. After pyrolysis, the composites were washed with methanol to remove any impurities and then dried at 60 °C to ensure complete removal of moisture before further characterisation and adsorption experiments.

CHARACTERIZATION OF ZnO-MPEW-NCs

FTIR Analysis

The FTIR (Figure 1) was used to identify the functional groups present in the ZnO-MPEW-NCs. The samples were mixed with potassium bromide (KBr) in a 1:100 ratio and pressed into thin pellets. The FTIR spectra were recorded using a Bruker Invenio R (Germany) spectrometer over a range of 4000-400 cm^{-1} with a resolution of 4 cm^{-1}. The resulting spectra provided information about the chemical bonding and surface functionalization of the composite material.

BET Analysis

The BET specific surface area (m^2/g), average pore size (nm), and average pore volume (m^3/g) of the prepared composite materials were obtained using the BET (Figure 2) with N_2 adsorption at -196 °C. The results were obtained using TriStarII Plus, Micromeritics GA USA version 2.03. Before the analysis was conducted, about 0.3 g of the sample was degassed for 8 h under vacuum at 200 °C until the gradient of pressure was low. The isotherms were generated as a result of dosing nitrogen gas onto the surface of the sample. The adsorption-desorption graph gives the details about the surface area and the average pore volume using the technique of BET from Figure 2. The pore size distribution was determined from the desorption part of the isotherm using the Barrett-Joyner-Halenda method.

FESEM Analysis

The FESEM (Figure 3) was used to assess surface morphology and elemental distribution. A Nova NanoSEM 230 microscope (Netherlands) was used for FESEM. Before imaging, the samples were coated with a conductive layer using a JEOL JFC-1600 auto fine coater. Imaging was carried out at 5 kV with a working distance of approximately 500 nm, an aperture setting of 3, and a magnification of up to 100,000×.

UV/Visible Spectroscopic Analysis (UV-Vis)

Before the adsorption experiments, the UV-Vis spectrum of the MNZ solution was recorded using a PerkinElmer Lambda 35 UV-Vis spectrophotometer (USA), at a wavelength range of 200 to 800 nm. The maximum absorbance of MNZ was observed at 320 nm. A calibration plot of the MNZ aqueous solution was performed at various concentrations ranging from 2 to 20 mg/L. The concentration of MNZ remaining in solution was determined by measuring the absorbance at 320 nm using a UV–Vis spectrophotometer and comparing the values with a previously established calibration curve. The MNZ removal efficiency and adsorption capacity were calculated using Equations (1) and (2).

$$\text{Removal efficiency (\%)} = (C_i - C_t / C_i) \times 100 \quad (1)$$

$$q_e = \frac{(C_i - C_t)}{m} \times V \quad (2)$$

where C_i and C_t (mg/L) are the concentrations of MNZ at time 0 and at time t, respectively; V (L) is the volume of the solution; and m (g) is the mass of the adsorbent. Adsorption kinetics serves as a tool to examine reaction rates, factors influencing these rates, and the transport behavior of particles in the adsorbed material. To achieve this, a reaction mixture containing MNZ at concentrations ranging from 2-20 mg/L was prepared, with contact times between 5-120 min, a pH of 7, and an adsorbent dose of 0.1 g/500 mL. Following the experiments, the removal efficiency of MNZ was evaluated.

KINETIC MODEL ANALYSIS

The kinetic models analyzed included pseudo-first-order, pseudo-second-order, and intraparticle diffusion equations. In the subsequent phase, adsorption isotherms were studied to understand how solute concentration impacts the adsorbent's performance. The pseudo-first-order is displayed as Equation (3).

$$\ln(q_e - q_t) = \ln q_e - k_1 \times t \quad (3)$$

where k_1($^1/min$) is the pseudo-first-order kinetic constant; q_e (mg/g), and q_t (mg/g) are the MNZ adsorption of ZnO-MPEW-NCs at time t, respectively. The pseudo-second-order kinetics is given in Equation (4).

$$t/q_t = 1/k_2 q_e^2 + (1/q_e)t \quad (4)$$

The pseudo-second-order model is characterized by its rate constant, k_2 (g/mg·min), and the adsorption capacities at equilibrium (q_e) and at any given time (q_t). The intra-particle diffusion model can be expressed in a linear form, as shown in Equation (5). This model is used to understand the rate at which the substance diffuses within the pores of the adsorbent. The equation typically takes the following form, given in Equation (5).

$$q_t = k_{id}\, t^{1/2} + C \quad (5)$$

where q_t is the amount of adsorbate adsorbed at time t (mg/g); k_{id} is the intraparticle diffusion rate constant (mg/g·min$^{1/2}$); and C is a constant related to the boundary layer thickness. This model helps determine the contribution of diffusion to the overall adsorption process.

ADSORPTION ISOTHERM MODELS

The Langmuir model assumes monolayer adsorption occurs on a uniform surface. Its equation defines parameters such as q_{max} (maximum adsorption capacity in mg/g), q_e (equilibrium adsorption capacity), and b (Langmuir constant in L/mg) as shown in Equation (6).

$$\frac{C_e}{q_e} = \frac{1}{q_{max}} C_e + \frac{1}{K_L q_{max}} \quad (6)$$

The Freundlich model accounts for surface heterogeneity and variations in adsorption energies from Equation (7), which are distributed exponentially (Yoosefian et al. 2017). Its formula defines q_e (adsorption capacity at equilibrium in mg/g) and K_f (Freundlich constant in L/g) (Nasoudari et al. 2023).

$$\ln q_e = \ln K_f + \left(\frac{1}{n}\right) \ln C_e \quad (7)$$

The Temkin isotherm considers the indirect interactions between adsorbate molecules during adsorption. It assumes that the heat of adsorption (ΔH^o) for all molecules in the layer decreases linearly as surface coverage increases. This model is most applicable to systems with moderate ionic strength. The linear form of the Temkin isotherm is given in Equation (8).

$$q_e = \frac{RT}{b} \ln K_t + \frac{RT}{b} \ln C_e \quad (8)$$

where q_e is the amount of adsorbate at equilibrium (mg/g); R is the universal gas constant (8.314 J/mol·K); T is the absolute temperature (K); and b is the Temkin constant related to the heat of sorption (J/mol); K_t is the Temkin isotherm constant (L/g); and C_e is the concentration of the adsorbate at equilibrium (mg/L). This equation provides insight into the relationship between the adsorbate concentration and its interaction with the adsorbent surface, especially in systems with intermediate ionic concentrations.

RESULTS AND DISCUSSION

CHARACTERIZATION OF ZnO-MPEW-NCs

FTIR Analysis of Functional Groups in ZnO-MPEW-NCs

The FTIR spectroscopy was employed to investigate the functional groups present in the ZnO-MPEW-NCs before and after thermal treatment Figure 1. The unheated sample (a) exhibited a broad band near 3430 cm^{-1} due to O-H stretching, indicating surface hydroxyl groups and moisture (Munir et al. 2024). Absorption bands at 2920 and 2850 cm^{-1} were assigned to asymmetric/symmetric C-H stretching, characteristic of PEW segments (Munir et al. 2024). A distinct band at around 1730 cm^{-1} corresponded to C=O stretching, likely from carbonyl groups in oxidized polymer chains (Ubaidullah et al. 2020). Vibrational signals in the range of 1450-1500 cm^{-1} showed C=C stretching, indicating partial degradation of polymeric structures (Chen et al. 2022). After thermal processing at 300-500 °C, the intensities of these organic bands decreased markedly, while the emergence of peaks around 1030 cm^{-1} (Si-O), 600-700 cm^{-1} (Zn-O stretching), and ~450 cm^{-1} (ZnO lattice vibrations) became more pronounced, confirming the formation and crystallization of ZnO phases (Synergy between activated carbon and ZnO) (Munir et al. 2024). The decrease in the FTIR band associated with the Si–O bond after pyrolysis can be attributed to partial decomposition and restructuring of silicon-containing species at elevated temperature. At 400-500 °C, the organic fraction is largely decomposed, and the inorganic Si–O network may undergo condensation, densification, or partial volatilization of silicon species, leading to weaker vibrational signals.

BET Nitrogen Adsorption–Desorption Analysis of ZnO-MPEW-NCs

The nitrogen adsorption–desorption isotherms of ZnO-MPEW-NCs (Figure 2) exhibit typical Type IV behavior with H3-type hysteresis loops, suggesting the presence of slit-like mesopores, a characteristic feature of thermally processed ZnO-carbon hybrid materials (Qin et al. 2023). The unpyrolyzed composite (sample a) displays a low BET surface area of 10 m²/g, a modest pore volume of 0.037 cm³/g, and an average pore diameter of 7.8 nm. Table 1 is indicative of a largely closed or polymer-dominated matrix with limited accessible porosity (Sedefoglu 2024). Upon pyrolysis at 300 °C (sample b), there is a marked increase in surface area to 32 m²/g and pore volume to 0.087 cm³/g, accompanied by a reduction in pore diameter to 5.5 nm. This can be attributed to the partial thermal

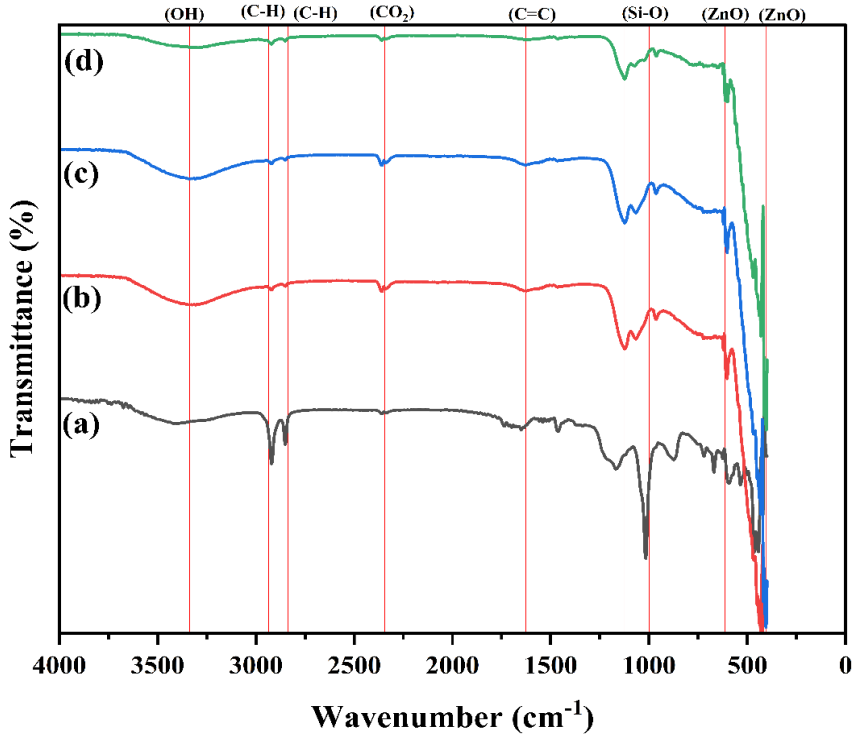

FIGURE 1. FTIR spectra of ZnO-MPEW-NCs: (a) unpyrolyzed, (b) pyrolyzed at 300 °C, (c) pyrolyzed at 400 °C, and (d) pyrolyzed at 500 °C

degradation of polymeric chains and the initial formation of mesoporous structures (Wan et al. 2023). At 400 °C (sample c), the BET surface area rises to 54 m^2/g, the pore volume increases to 0.134 cm^3/g, and the average pore diameter narrows further to 4.7 nm (Table 1), reflecting the progression of carbonization and the enhancement of porosity within the composite framework. The most significant improvement is observed at 500 °C (sample d), where the BET surface area peaks at 106 m^2/g, pore volume reaches 0.260 cm^3/g, and the average pore diameter decreases to 3.9 nm (Table 1), indicating optimal mesopore development resulting from the complete decomposition of organics and restructuring of the ZnO-carbon matrix (Wan et al. 2023). This progressive thermal activation and pore evolution align with recent studies showing that increasing the pyrolysis temperature of polymer–metal oxide systems significantly enhances surface textural properties, thereby improving their adsorption efficiency for environmental remediation applications (Qin et al. 2023).

FESEM and Particle Size Distribution Analysis of ZnO-MPEW-NCs

Figure 3(a)-3(d)) illustrates the particle size distribution alongside FESEM images of ZnO-MPW-NCs after undergoing various thermal treatments. The unpyrolyzed ZnO-MPEW-NCs sample (Figure 3(a)) has an average particle size of 36.67 nm, featuring relatively uniform and distinct particles with little agglomeration. The FESEM image displays a uniformly dispersed nanostructure, suggesting a well-integrated ZnO phase within the PEW matrix (Sedefoglu 2024). When subjected to thermal treatment at 300 °C (Figure 3(b)), the average particle size grows to 42.25 nm. This increase is linked to the beginning of thermally driven coalescence and grain boundary migration, as shown by the clearer particle aggregates in the FESEM image (Jadhav et al. 2024). Heating further to 400 °C (Figure 3(c)) leads to a notable rise in particle size to 54.21 nm. The resulting FESEM micrograph indicates more evident signs of particle fusion and densification, suggesting that higher thermal energy promotes enhanced crystallite growth (Rabbani et al. 2021). At 500 °C (Figure 3(d)), the ZnO-MPEW-NCs exhibit the largest average particle size of 56.72 nm. The FESEM image shows considerable particle aggregation along with reduced surface roughness, which is characteristic of sintering effects often observed at elevated calcination temperatures. These morphological alterations correspond with thermally activated diffusion and recrystallization mechanisms, promoting the development of larger, denser grains (Rabbani et al. 2021).

ADSORPTION OF MNZ ONTO ZnO-MPEW-NCs

Kinetic Analysis of MNZ Adsorption onto ZnO-MPEW-NCs

The adsorption kinetics of MNZ onto ZnO-MPEW-NCs synthesized at different pyrolysis temperatures were investigated to understand the adsorption rate and mechanism (Figure 4). Among all tested materials, the

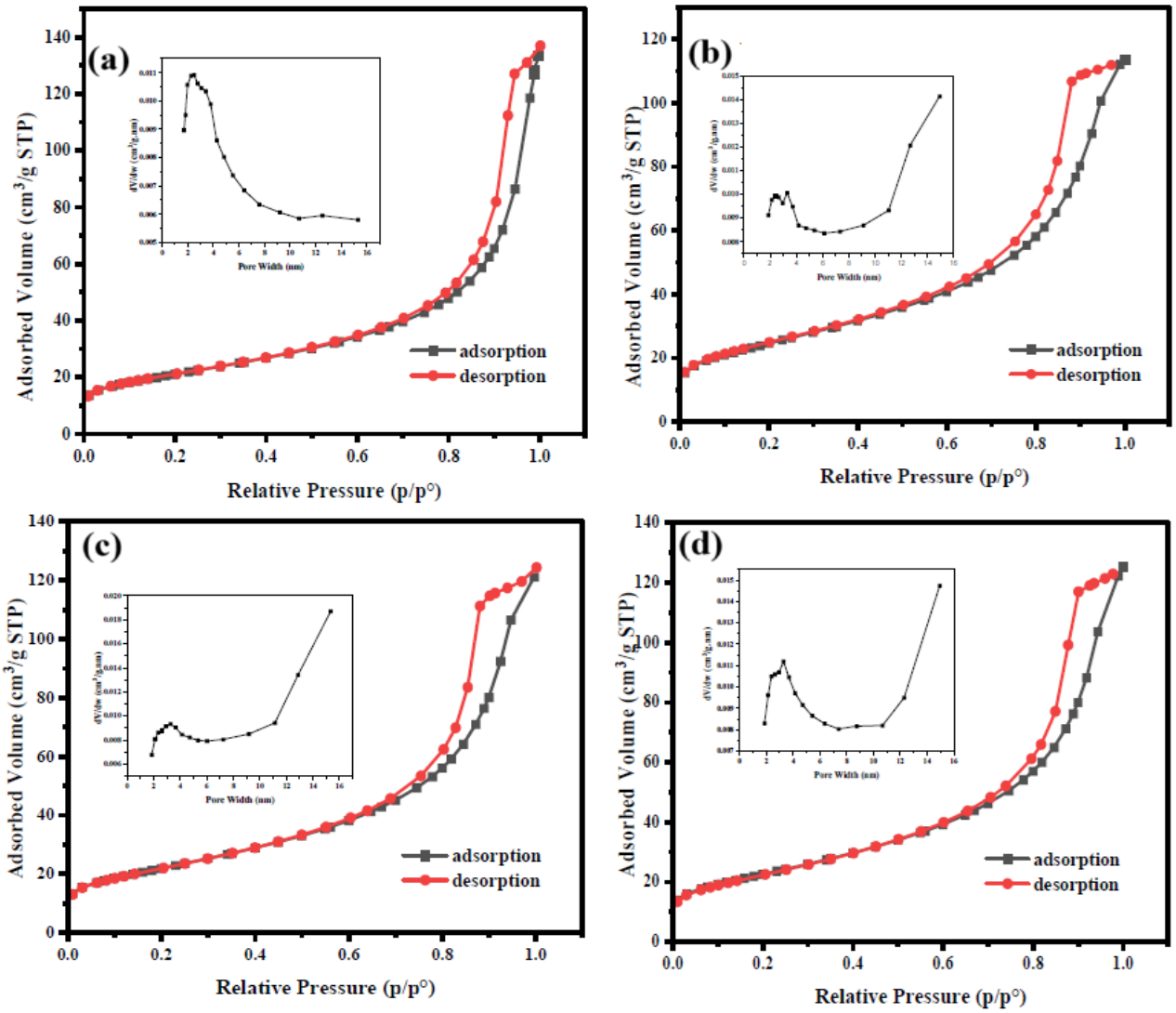

FIGURE 2. Nitrogen adsorption–desorption isotherms of samples ZnO-MPEW-NCs: (a) unpyrolyzed, (b) pyrolyzed at 300 °C, (c) pyrolyzed at 400 °C, and (d) pyrolyzed at 500 °C, measured at 77 K. Pore size distributions (insets) were obtained from the desorption branch using the Barrett–Joyner–Halenda (BJH) method

TABLE 1. BET surface area, pore size, and pore volume distribution of ZnO-MPEW-NCs: (a) unpyrolyzed, (b) pyrolyzed at 300 °C, (c) pyrolyzed at 400 °C, and (d) pyrolyzed at 500 °C

Sample	BET surface area (m^2/g)	Pore volume (m^3/g)	Pore size BJH (nm)
(a)	10	0.037	7.8
(b)	32	0.087	5.5
(c)	54	0.134	4.7
(d)	106	0.260	3.9

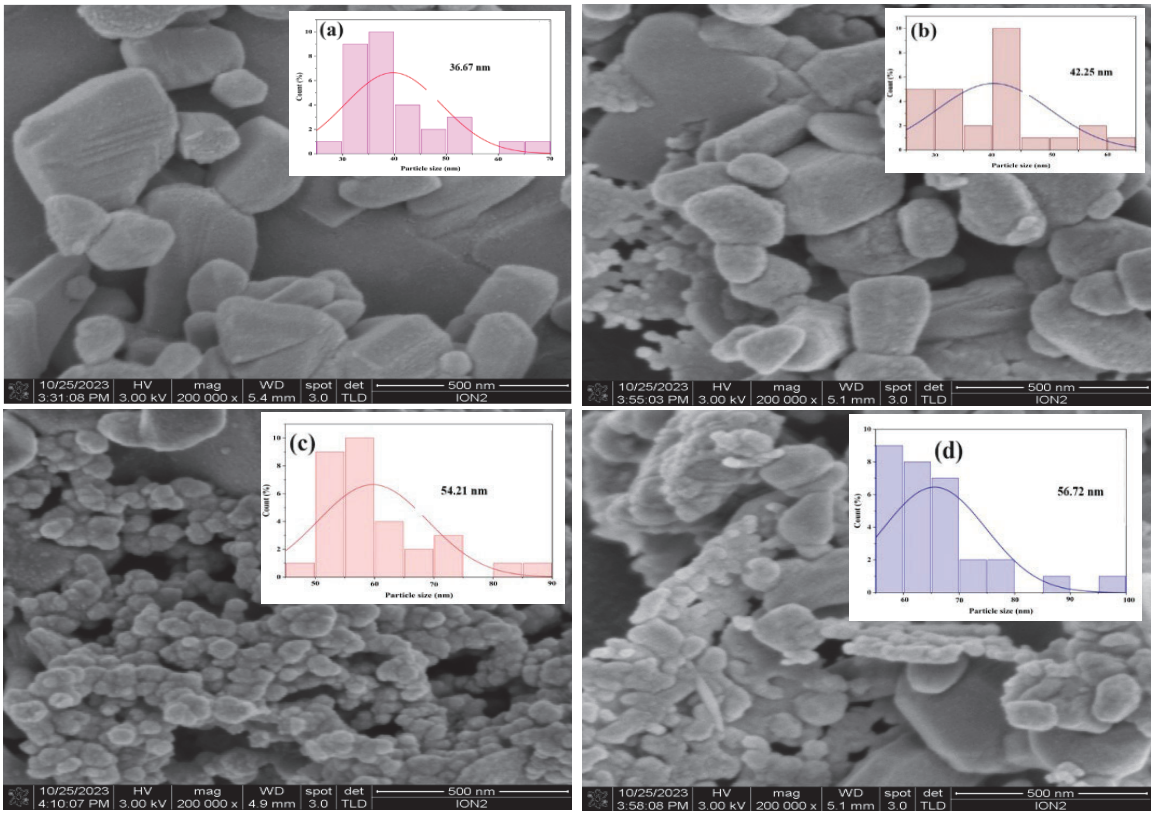

FIGURE 3. FESEM images and average particle size distribution of ZnO-MPEW-NCs: (a) unpyrolyzed, (b) pyrolyzed at 300 °C, (c) pyrolyzed at 400 °C, and (d) pyrolyzed at 500 °C

composite pyrolyzed at 500 °C exhibited the highest adsorption performance. Removal efficiency increased progressively with contact time, reaching equilibrium after 30 min, with a maximum adsorption capacity of 9.94 mg/g and a removal efficiency of 99.4%, indicating rapid and effective adsorption. The experimental data were fitted to three kinetic models: pseudo-first-order, pseudo-second-order, and intraparticle diffusion. The kinetic parameters and model equations are summarized in Table 2. Comparative analysis of correlation coefficients (R^2), theoretical adsorption capacities (q_{cal}), and chi-square (χ^2) values showed that the pseudo-second-order model best described the adsorption kinetics, with $R^2 = 0.99941$ and $q_{cal} = 9.88$ mg/g, closely matching the experimental value. The pseudo-first-order model provided a slightly lower correlation ($R^2 = 0.99934$) and underestimated the adsorption capacity ($q_{cal} = 5.575$ mg/g), indicating it is less suitable for describing the adsorption behavior.

Intraparticle diffusion analysis further showed a biphasic pattern (Figure 4), with an initial rapid adsorption stage corresponding to surface interactions, followed by a slower phase associated with diffusion within the pores. The intraparticle diffusion rate constant (k_{id}) was highest for the 500 °C-pyrolyzed sample (3.572 mg/g·min$^{1/2}$), suggesting that pyrolysis at this temperature improves surface area, pore structure, and active site accessibility, facilitating faster diffusion and higher adsorption efficiency (Awual et al. 2023). Overall, the kinetic results indicate that MNZ adsorption on ZnO-MPEW-NCs is rapid and primarily governed by physisorption, with contributions from both surface adsorption and intraparticle diffusion. The pseudo-second-order model accurately describes the kinetics.

The adsorption of MNZ onto ZnO-MPEW-NCs is primarily governed by hydrogen bonding, electrostatic interactions, and surface complexation mechanisms. As illustrated in Figure 5, MNZ molecules contain nitro (–NO_2), hydroxyl (–OH), and imidazole functional groups that can interact with surface (–OH), groups and oxygen (–O_2), -containing functionalities present on the ZnO-MPEW-NCs. The incorporation of ZnO nanoparticles (ZnO-NPs) provides positively charged Zn^{2+} active sites and abundant surface –OH groups, which facilitate coordination and electrostatic attraction with electron-donating groups of MNZ. Furthermore, under suitable pH conditions, electrostatic interactions between ionized MNZ species and the adsorbent surface are enhanced, leading to increased adsorption affinity. In addition, the porous carbonaceous framework derived from pyrolyzed mixed MPEW, as evidenced by the structural features shown in Figure 3, promotes pore diffusion and physical entrapment of MNZ molecules, resulting in improved adsorption capacity and stability.

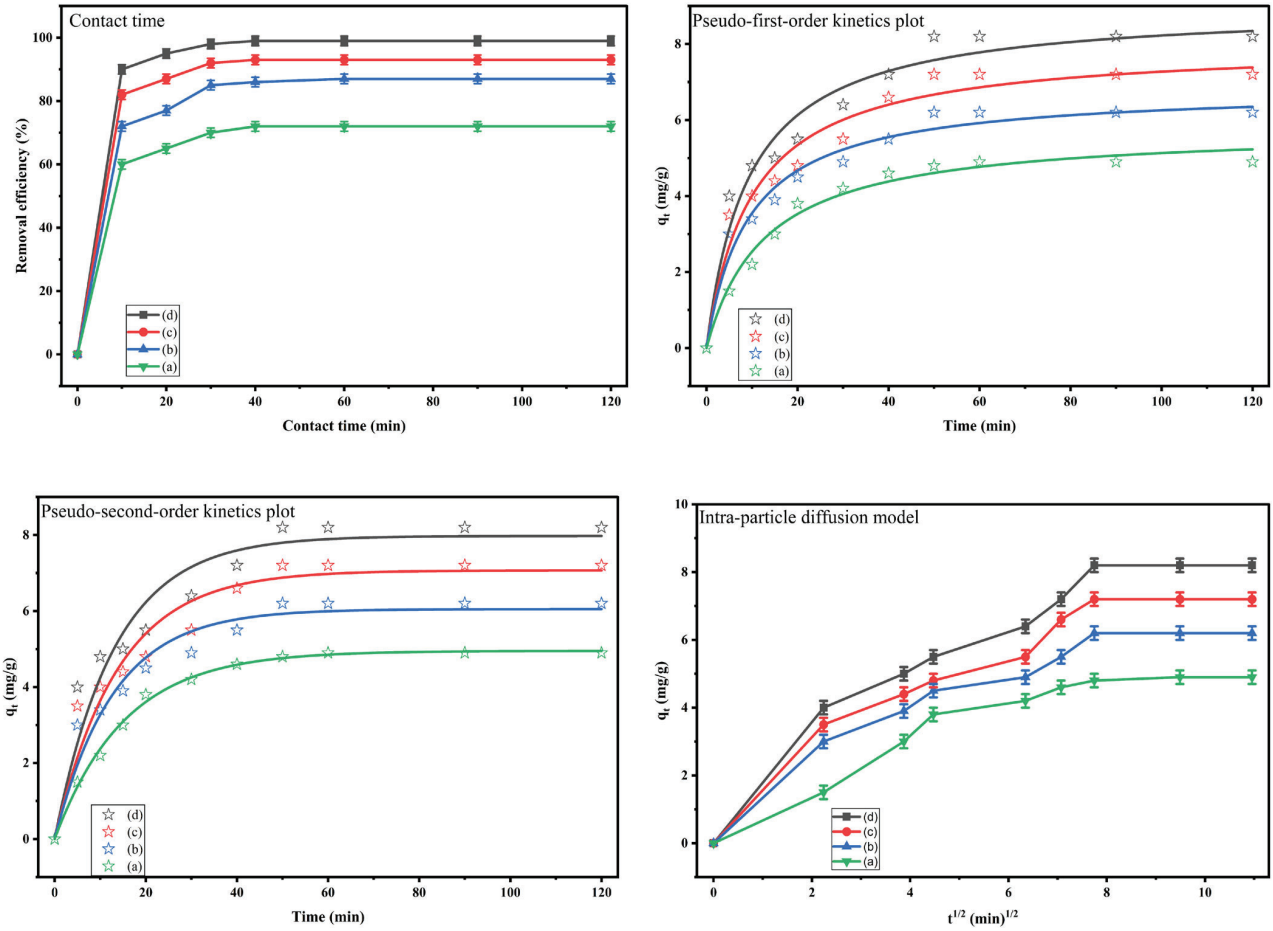

FIGURE 4. Effect of contact time, pseudo-first-order, pseudo-second-order kinetics, and intra-particle diffusion on MNZ adsorption by ZnO-MPEW-NCs under different pyrolysis conditions (experimental conditions: adsorbent dose = 0.1 g/500 mL; initial MNZ concentration = 2 mg/L; 25 °C; pH = 7)

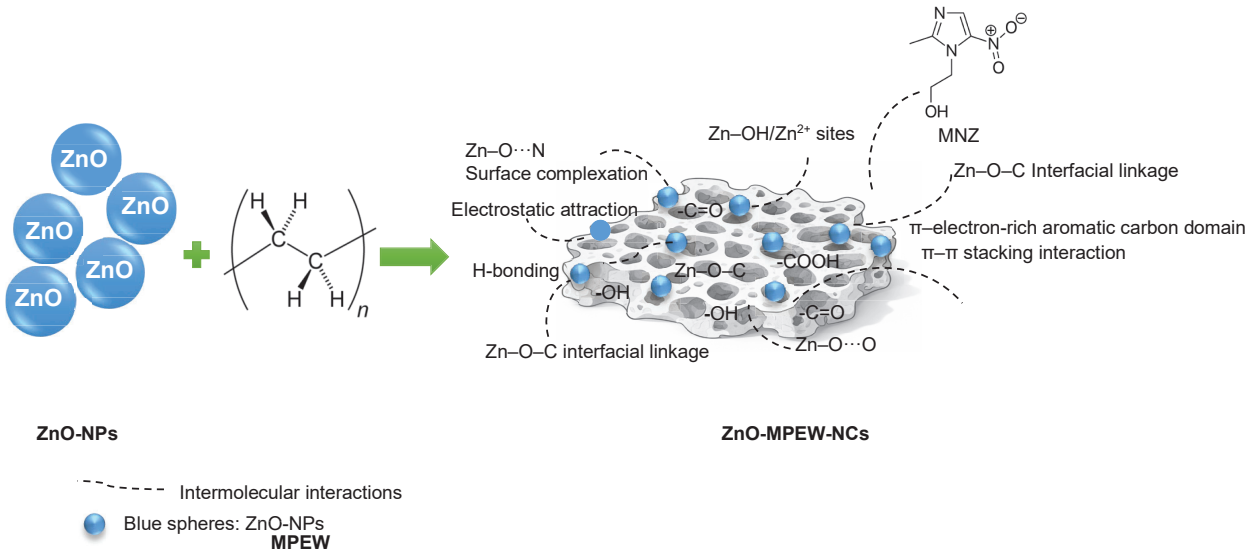

FIGURE 5. Proposed interaction mechanism between ZnO-MPEW-NCs with MNZ

TABLE 2. Kinetic adsorption models for MNZ adsorption onto ZnO-MPEW-NCs: (a) unpyrolyzed, (b) pyrolyzed at 300 °C, (c) pyrolyzed at 400 °C, and (d) pyrolyzed at 500 °C

Parameters	Sample (a)	Sample (b)	Sample (c)	Sample (d)
Pseudo-first-order kinetic model				
q_e (exp.)	8.60	9.20	9.66	9.99
k_i(1/min)	0.00221	0.00442	0.00887	0.01234
q_e(cal.)	0.655	2.32	3.488	5.575
R^2	0.99361	0.99443	0.9968	0.99934
Chi-square (χ^2)	96.37	20.40	10.92	3.50
Pseudo-second-order kinetic model				
q_e (exp.)	8.60	9.20	9.66	9.99
k_2 (g/(mg.min)	0.33	0.38	0.57	0.99
q_e(cal.)	8.54	9.11	9.55	9.88
R^2	0.99629	0.99459	0.9982	0.99941
Chi-square (χ^2)	0.00042	0.00089	0.00127	0.00122
Intra-particle diffusion model				
K_{id}(mg.min$^{1/2}$/g)	2.73	3.17	3.38	3.58
C_i (mg/g)	0.82	0.63	0.44	0.22
R^2	0.87661	0.90821	0.91223	0.93221

Impact of Initial MNZ Concentration on the Adsorption Efficiency of ZnO-MPEW-NCs

Figure 6 illustrates the influence of varying initial MNZ concentrations on the adsorption performance of ZnO-MPEW-NCs. The data indicate that the removal efficiency decreases as the MNZ concentration increases, with efficiencies of 99.5%, 97%, 94%, 90%, and 87% for concentrations of 2, 5, 10, 15, and 20 mg/L, respectively. The highest removal efficiency of 99.5% was observed at 2 mg/L. This trend can be attributed to the availability of active adsorption sites on the composite surface. At lower pollutant concentrations, a greater number of vacant active sites and a higher generation of reactive radicals promote efficient MNZ uptake. However, as the concentration of MNZ increases, these active sites gradually become saturated. The elevated molecular load and increased turbidity hinder further adsorption, leading to a decline in removal efficiency. The reduced performance at higher concentrations is primarily attributed to the exhaustion of accessible surface sites and potential pore blockage, which limits the diffusion and interaction of MNZ molecules with the composite surface (Lotfi Golsefidi, Zahmatkesh Anbarani & Bonyadi 2023).

Adsorption Isotherm Analysis of MNZ on ZnO-MPEW-NCs

The adsorption equilibrium of MNZ onto ZnO-MPEW-NCs pyrolyzed at 500 °C was systematically evaluated using the Langmuir, Freundlich, and Temkin isotherm models to elucidate the adsorption mechanism and surface characteristics. The Langmuir and the Freundlich isotherm plots are presented in Figure 7. The Langmuir model, which assumes monolayer adsorption on a homogeneous surface, yielded a maximum adsorption capacity (q_{max}) of 133.75 mg/g and a dimensionless separation factor (R_L) of 0.114, confirming favorable adsorption under the investigated conditions (Mozaffari & Bodaghifard 2024).

The Freundlich model, which describes adsorption on heterogeneous surfaces with possible multilayer formation, provided the best fit to the experimental data ($R^2 = 0.99814$) compared to the Langmuir model ($R^2 = 0.98048$), as shown in Figure 7. This superior fit indicates that MNZ adsorption predominantly occurs on a heterogeneous surface with multilayer coverage, consistent with the structural and surface complexity of the ZnO-MPEW-NCs after pyrolysis at 500 °C. Moreover, the Freundlich adsorption intensity parameter ($n > 1$) further confirms the favorable nature of the adsorption process.

The Temkin isotherm model, illustrated in Figure 8, accounts for adsorbate–adsorbent interactions and a linear decrease in adsorption heat with increasing surface coverage. This model also showed a strong correlation with the experimental data. The Temkin constants for the 500 °C-pyrolyzed material ($b = 10.601$ kj/mol and $A = 8.264$ L/g) were higher than those of the unpyrolyzed sample, indicating enhanced interaction strength between MNZ molecules and the adsorbent surface. Notably, the Temkin b value (< 40 kJ/mol) suggests that the adsorption process is predominantly governed by physisorption mechanisms (Cao et al. 2021).

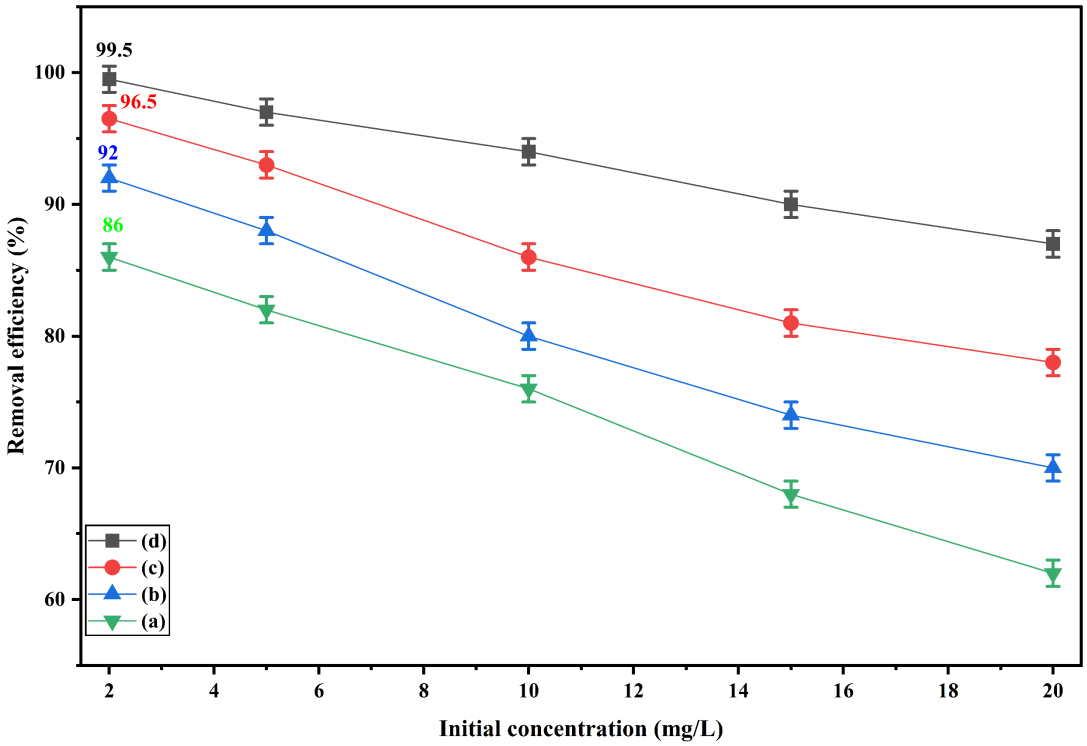

FIGURE 6. Effect of initial MNZ concentration on adsorption by ZnO-MPEW-NCs under different pyrolysis conditions: (a) unpyrolyzed, (b) pyrolyzed at 300 °C, (c) pyrolyzed at 400 °C, and (d) pyrolyzed at 500 °C (experimental conditions: adsorbent dose = 0.1 g/500 mL; temperature = 25 °C; pH = 7)

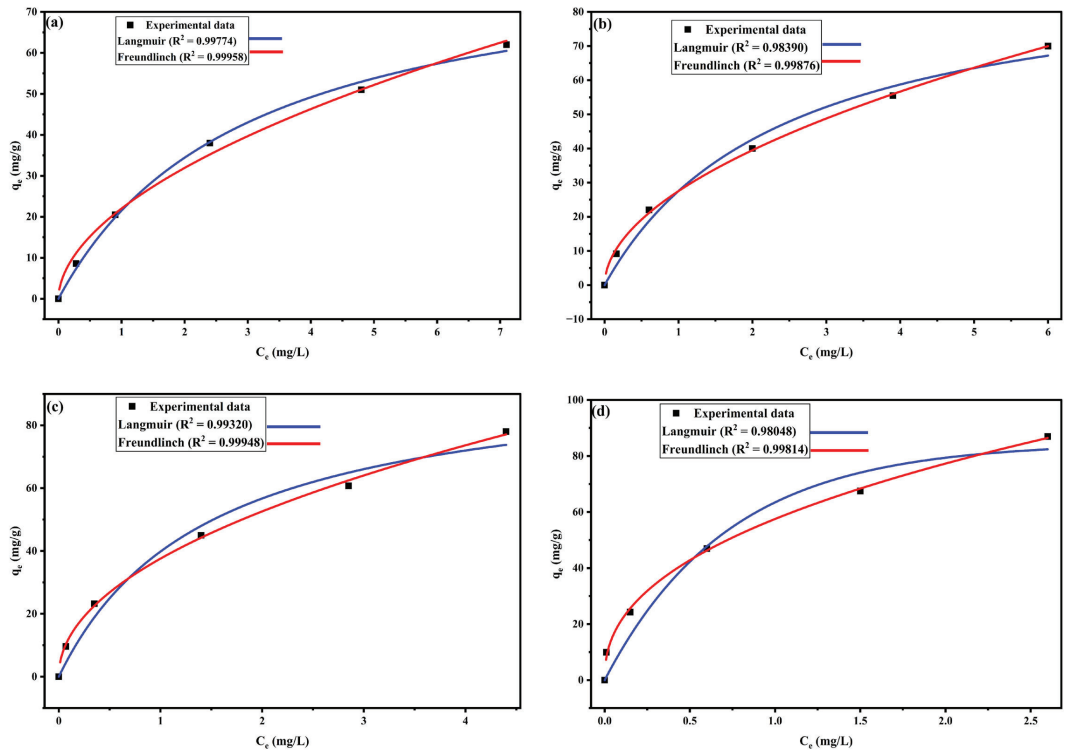

FIGURE 7. Non-linear Langmuir and Freundlich isotherm model fits for ZnO-MPEW-NCs under different pyrolysis conditions: (a) unpyrolyzed, (b) pyrolyzed at 300 °C, (c) pyrolyzed at 400 °C, and (d) pyrolyzed at 500 °C

Overall, the isotherm analysis demonstrates that ZnO-MPEW-NCs pyrolyzed at 500 °C exhibit significantly enhanced adsorption performance toward MNZ, characterized by multilayer adsorption on heterogeneous surfaces dominated by physical interactions. These results highlight the strong potential of these nanocomposites as efficient adsorbents for the environmental remediation of pharmaceutical contaminants.

Temperature Dependence of MNZ Adsorption on ZnO-MPEW-NCs: A Thermodynamic Study

The effect of temperature on the adsorption efficiency of MNZ onto ZnO-MPW-NCs was systematically evaluated at 298 K, 308 K, and 313 K. As illustrated in Figure 9, the removal efficiency of the nanocomposite decreased slightly from 99.2% at 298 K to 94.6% at 313 K. This marginal reduction suggests that the adsorption process exhibits weak temperature dependence, indicating a predominantly physical adsorption mechanism (Mozaffari & Bodaghifard 2024). To gain further insight into the thermodynamic nature of the adsorption, the ΔG°, ΔH°, and ΔS° were calculated using established thermodynamic relationships (Mozaffari & Bodaghifard 2024). The distribution coefficient (K_d) was calculated according to Equation (9).

$$K_d = q_e / C_e \tag{9}$$

where q_e is the amount of adsorbate adsorbed at equilibrium (mg/g); and C_e is the equilibrium concentration (mg/L). A linear van't Hoff plot was constructed by plotting ln K_d against 1/T, as described by Equation (10):

$$\ln K_d = (\Delta S° / R) - (\Delta H° / RT) \tag{10}$$

Here, R is the universal gas constant (8.314 J/mol·K), and T represents the absolute temperature in Kelvin. The values of ΔH° and ΔS° were obtained from the slope and intercept of the linear plot, respectively. Subsequently, the standard Gibbs free energy change at each temperature was calculated using Equation (11):

$$\Delta G° = \Delta H° - T\Delta S° \tag{11}$$

The negative values of ΔG° across the investigated temperature range (298-313 K) confirm that the adsorption of MNZ onto the ZnO-MPEW-NCs is a spontaneous process. Moreover, the decrease in ΔG° magnitude with increasing temperature indicates that adsorption is thermodynamically more favorable at lower temperatures, as summarized in Table 6. The observed negative ΔH° value suggests that the adsorption process is exothermic (Mozaffari & Bodaghifard 2024). Conversely, the negative ΔS° value indicates a decrease in disorder at the solid-liquid interface during the adsorption process. This reduction in randomness may limit molecular mobility and interactions, but the system reaches equilibrium more quickly at lower temperatures, as evidenced by the short equilibrium time (Abid et al. 2025).

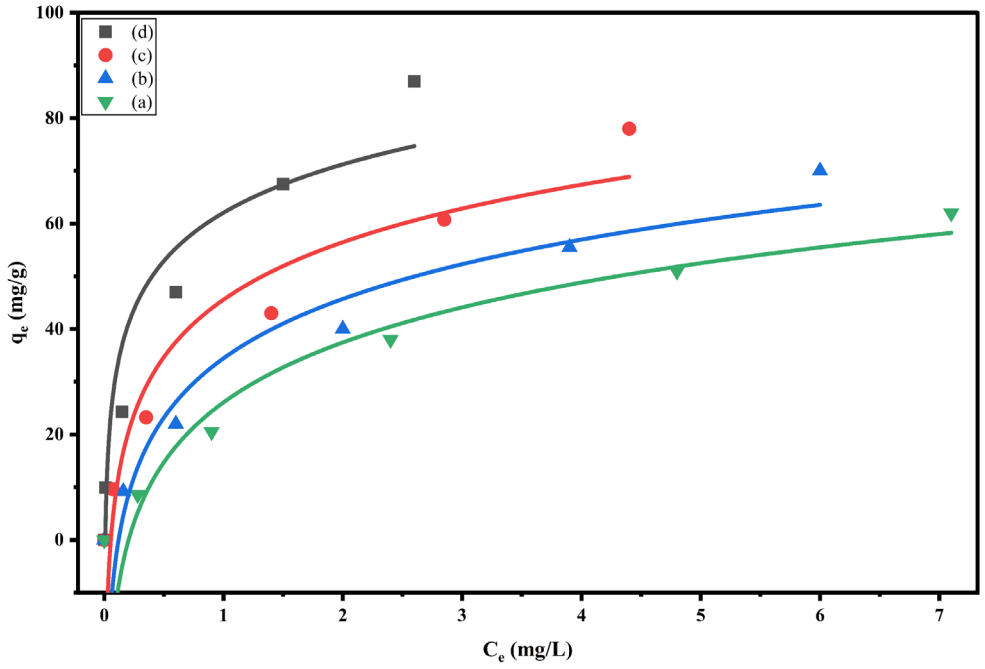

FIGURE 8. Non-linear Temkin isotherm model fit for ZnO-MPEW-NCs under different pyrolysis conditions: (a) unpyrolyzed, (b) pyrolyzed at 300 °C, (c) pyrolyzed at 400 °C, and (d) pyrolyzed at 500 °C (experimental conditions: adsorbent dose = 0.1 g/500 mL; initial MNZ concentration = 2 mg/L; temperature = 25 °C; pH = 7)

TABLE 3. Isotherm adsorption model parameters for MNZ adsorption onto ZnO-MPEW-NCs: (a) unpyrolyzed, (b) pyrolyzed at 300 °C, (c) pyrolyzed at 400 °C, and (d) pyrolyzed at 500 °C

Parameters	Sample (a)	Sample (b)	Sample (c)	Sample (d)
Langmuir isotherm				
q_e (mg/g)	66.54	86.21	105.58	133.75
K_L(L/mg)	1.433	1.872	2.454	3.880
R_L(cal.)	0.259	0.211	0.169	0.114
R^2	0.99774	0.98390	0.99320	0.98048
Chi-square (χ^2)	15.84	2.70	3.11	3.22
Freundlich isotherm				
K_F(mg/g)	10.22	22.65	33.78	57.21
n	1.68	2.29	2.78	4.55
R^2	0.99958	0.99876	0.99948	0.99814
Chi-square (χ^2)	2.22	1.44	0.77	0.12
Termkin				
b (kJ/mol)	8.201	8.874	9.480	10.601
A_T	1.135	2.896	4.232	8.264
R^2	0.97684	0.99121	0.96586	0.97458
Chi-square (χ^2)	2038.88	240.75	224.04	176.40

TABLE 6. Thermodynamic parameters of MNZ adsorption onto ZnO-MPEW-NCs: (a) unpyrolyzed, (b) pyrolyzed at 300 °C, (c) pyrolyzed at 400 °C, and (d) pyrolyzed at 500 °C (adsorbent dose = 0.1 g/500 mL; initial MNZ concentration = 2 mg/L; pH = 7)

Sample	T(K)	ΔG° (kJ/mol)	ΔH° (kJ/mol)	ΔS° (J/(mol.K))
(a)	298	-2.90	-10.50	-25.5
	308	-2.65		
	318	-2.39		
(b)	298	-3.74	-15.66	-40.0
	308	-3.34		
	318	-2.94		
(c)	298	-7.87	-26.05	-60.56
	308	-7.26		
	318	-6.65		
(d)	298	-12.48	-42.88	-102.0
	308	-11.64		
	318	-10.44		

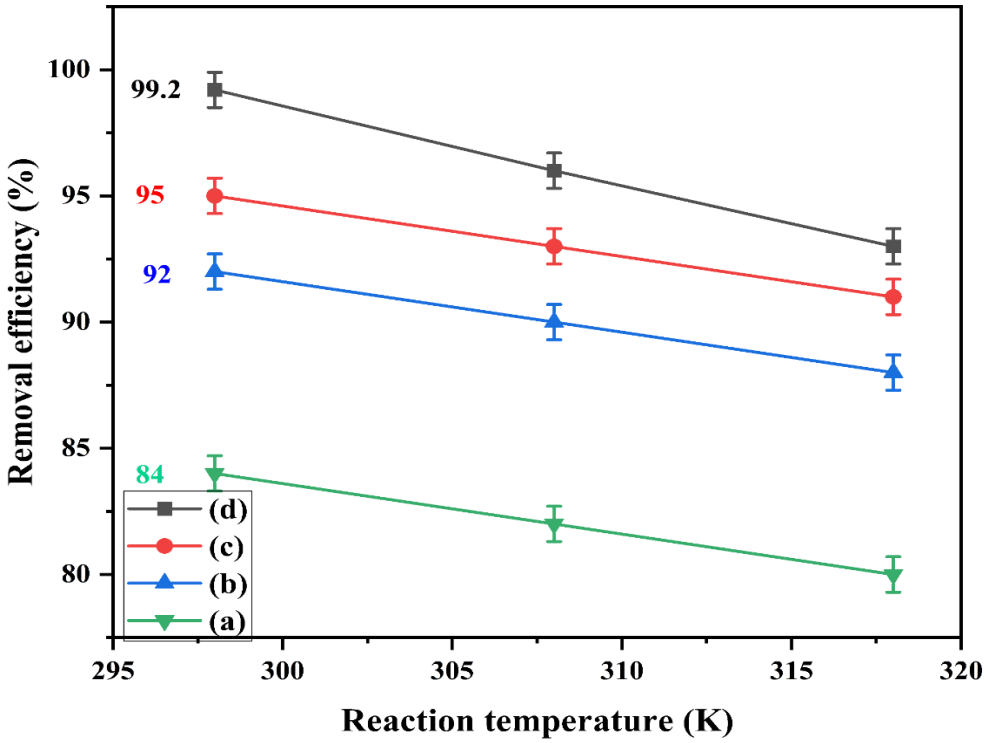

FIGURE 9. Effect of temperature on MNZ adsorption onto ZnO-MPEW-NCs: (a) unpyrolyzed, (b) pyrolyzed at 300 °C, (c) pyrolyzed at 400 °C, and (d) pyrolyzed at 500 °C (experimental conditions: adsorbent dose = 0.1 g/500 mL; initial MNZ concentration = 2 mg/L; pH = 7)

CONCLUSION

This study successfully synthesized ZnO-MPEW-NCs, and characterization analyses (FTIR, SEM, and BET) confirmed their structural modification, chemical stability, and enhanced surface area, increasing from 10 to 106 m^2/g after pyrolysis at 500 °C. The adsorption of MNZ, a widely used antibiotic and emerging water contaminant, onto these nanocomposites was rapid, reaching equilibrium within 30 min. The 500 °C-pyrolyzed sample exhibited the highest adsorption capacity (133.75 mg/g) and removal efficiency (99.4%). Kinetic studies demonstrated that the pseudo-second-order model (R^2 = 0.99941, q_{cal} = 9.88 mg/g) best described the adsorption process, while intraparticle diffusion analysis indicated contributions from both surface interactions and pore diffusion. Equilibrium data fit the Freundlich isotherm (R^2 = 0.99958), confirming multilayer adsorption on a heterogeneous surface dominated by physisorption. Thermodynamic analysis further showed that the adsorption process was spontaneous and exothermic ($\Delta G°$ = −2.90 to 10.44 kJ/mol, $\Delta H°$ = −10.50 to −42.88 kJ/mol, and $\Delta S°$ = −25.5 to −102 J/(mol. K)), consistent with physical adsorption mechanisms. By acknowledging and quantifying the chemical byproducts generated during activation, this study provides a more transparent and realistic assessment of ZnO-MPEW-NCs production compared with earlier studies that overlook secondary waste streams. These findings demonstrate that ZnO-MPEW-NCs, particularly those pyrolyzed at 500 °C, are effective and sustainable adsorbents for removing pharmaceutical contaminants from water, addressing environmental and public health concerns, and advancing practical strategies for water remediation.

ACKNOWLEDGMENTS

We gratefully acknowledge the Research Management Centre (RMC) of Universiti Putra Malaysia (UPM) for funding this research under Geran Putra (Geran Putra Berimpak), UPM (grant code: UPM.RMC.800-3/3/1/GP-GPB/2021/9699200). We also like thank the Chemistry Department, Faculty of Science, Universiti Putra Malaysia, for the research facilities and technical support.

REFERENCES

Alamgir, Talha, K., Wang, B., Liu, J.H., Ullah, R., Feng, F., Yu, J., Chen, S. & Li, J.R. 2020. Effective adsorption of metronidazole antibiotic from water with a stable Zr(IV)-MOFs: Insights from DFT, kinetics and thermodynamics studies. *Journal of Environmental Chemical Engineering* 8(1): 103642. https://doi.org/10.1016/J.JECE.2019.103642

Arienzo, M. & Donadio, C. 2023. Microplastic–pharmaceuticals interaction in water systems. *Journal of Marine Science and Engineering* 11(7): 1437. https://doi.org/10.3390/JMSE11071437

Awual, M.R., Hasan, M.N., Hasan, M.M., Salman, M.S., Sheikh, M.C., Kubra, K.T., Islam, M.S., Marwani, H.M., Islam, A., Khaleque, M.A., Waliullah, R.M., Hossain, M.S., Rasee, A.I., Rehan, A.I. & Awual, M.E. 2023. Green and robust adsorption and recovery of Europium(III) with a mechanism using hybrid donor conjugate materials. *Separation and Purification Technology* 319: 124088. https://doi.org/10.1016/J.SEPPUR.2023.124088

Bashiri, F., Khezri, S.M., Kalantary, R.R. & Kakavandi, B. 2020. Enhanced photocatalytic degradation of metronidazole by TiO_2 decorated on magnetic reduced graphene oxide: Characterization, optimization and reaction mechanism studies. *Journal of Molecular Liquids* 314: 113608. https://doi.org/10.1016/J.MOLLIQ.2020.113608

Browne, A.J., Chipeta, M.G., Haines-Woodhouse, G., Kumaran, E.P.A., Hamadani, B.H.K., Zaraa, S., Henry, N.J., Deshpande, A., Reiner, R.C., Day, N.P.J., Lopez, A.D., Dunachie, S., Moore, C.E., Stergachis, A., Hay, S.I. & Dolecek, C. 2021. Global antibiotic consumption and usage in humans, 2000–18: A spatial modelling study. *The Lancet Planetary Health* 5(12): e893-e904. https://doi.org/10.1016/S2542-5196(21)00280-1

Cao, Y., Jiang, S., Zhang, Y., Xu, J., Qiu, L. & Wang, L. 2021. Investigation into adsorption characteristics and mechanism of atrazine on nano-MgO modified fallen leaf biochar. *Journal of Environmental Chemical Engineering* 9(4): 105727. https://doi.org/10.1016/J.JECE.2021.105727

Chen, Y., Li, Y., Luo, N., Shang, W., Shi, S., Li, H., Liang, Y. & Zhou, A. 2022. Kinetic comparison of photocatalysis with H_2O_2-free photo-fenton process on $BiVO_4$ and the effective antibiotic degradation. *Chemical Engineering Journal* 429: 132577. https://doi.org/10.1016/J.CEJ.2021.132577

Es'hagi, M., Farbodi, M., Gharbani, P., Ghasemi, E., Jamshidi, S., Majdan-Cegincara, R., Mehrizad, A., Seyyedi, K. & Shahverdizadeh, G.H. 2024. A comparative review on the mitigation of metronidazole residues in aqueous media using various physico-chemical technologies. *Analytical Methods* 16(43): 7294-7310. https://doi.org/10.1039/D4AY01502A

Habibi, M., Habibi-Yangjeh, A. & Khataee, A. 2023. S-scheme CeO_2-x/$AgFeO_2$/Ag photocatalysts with impressive activity in degradation of different antibiotics under visible light. *Surfaces and Interfaces* 39: 102937. https://doi.org/10.1016/J.SURFIN.2023.102937

Hazan, M.A., Chan, K.F., Jofri, K.A., Mamat, M.S., Endot, N.A., Liza, S., Ismail, I., Hussein, M.Z., Tanemura, M. & Yaakob, Y. 2021. Waste NR latex based-precursors as carbon source for CNTs eco-fabrications. *Polymers* 13(19): 3409. https://doi.org/10.3390/POLYM13193409

Hirata, Y., Kondo, H. & Ozawa, Y. 2014. Natural rubber (NR) for the tyre industry. In *Chemistry, Manufacture and Applications of Natural Rubber,* edited by Kohjiya, S. & Ikeda, Y. Woodhead Publishing. pp. 325-352. https://doi.org/10.1533/9780857096913.2.325

Jamshidi, E., Fathabadi, F., Manteghi, F. & Eshaghimalekshah, R. 2025. Adsorption characteristics of metronidazole on CoZr-LDH and its GO nanocomposite: Experimental and theoretical study. *Heliyon* 11(3): e42396. https://doi.org/10.1016/J.HELIYON.2025.E42396/ASSET/D166DF2A-664D-4B19-AC5C-F8C02929327F/MAIN.ASSETS/GA1.JPG

Lee, J.E., Lee, D., Lee, J. & Park, Y.K. 2025. Current methods for plastic waste recycling: Challenges and opportunities. *Chemosphere* 370: 143978. https://doi.org/10.1016/J.CHEMOSPHERE.2024.143978

Ling, X., Zheng, H., Huang, J., Sun, H., Xu, S., Zeng, H., Cai, A., Wang, Q. & Deng, J. 2024. The novel application of polyoxometalates for achieving sludge deep dewatering using low-temperature thermal hydrolysis pretreatment. *Journal of Cleaner Production* 444: 141125. https://doi.org/10.1016/J.JCLEPRO.2024.141125

Liu, Z., Xu, Z., Zhu, X., Yin, L., Yin, Z., Li, X. & Zheng, W. 2024. Calculation of carbon emissions in wastewater treatment and its neutralization measures: A review. *Science of The Total Environment* 912: 169356. https://doi.org/10.1016/J.SCITOTENV.2023.169356

Lotfi Golsefidi, F., Zahmatkesh Anbarani, M. & Bonyadi, Z. 2023. Removal of metronidazole antibiotic by modified red mud from aqueous solutions: Process modeling, kinetic, and isotherm studies. *Applied Water Science* 13(10): 202. https://doi.org/10.1007/S13201-023-01991-6/TABLES/8

Mashile, G.P., Mpupa, A., Nqombolo, A., Dimpe, K.M. & Nomngongo, P.N. 2020. Recyclable magnetic waste tyre activated carbon-chitosan composite as an effective adsorbent rapid and simultaneous removal of methylparaben and propylparaben from aqueous solution and wastewater. *Journal of Water Process Engineering* 33: 101011. https://doi.org/10.1016/J.JWPE.2019.101011

Mazloomi, S., Amarloei, A., Gholami, F., Haghighat, G.A., Badalians Gholikandi, G., Nourmoradi, H., Mohammadi, A.A., Fattahi, M. & Nguyen Le, B. 2023. Parametric study and process modeling for metronidazole removal by rhombic dodecahedron ZIF-67 crystals. *Scientific Reports* 13(1): 14654. https://doi.org/10.1038/s41598-023-41724-y

Mozaffari, F. & Bodaghifard, M.A. 2024. Synthesis of an O,N-rich porous organic polymer: Efficient removal of metronidazole from aqueous solutions. *Polymer Bulletin* 82(7): 2351-2372. https://doi.org/10.1007/S00289-024-05626-X/METRICS

Muhammad Aliyu, Abdul Halim Abdullah & Mohamed Ibrahim bin Mohamed Tahir. 2022. Adsorption tetracycline from aqueous solution using a novel polymeric adsorbent derived from the rubber waste. *Journal of the Taiwan Institute of Chemical Engineers* 136: 104333. https://doi.org/10.1016/J.JTICE.2022.104333

Munir, H.M.B., Yasin, S., Iqbal, T., Qamar, S., Ahmad, A., Mahmood, H. & Moniruzzaman, M. 2024. Thermomechanical evaluation of zinc oxide/hydroxyapatite/high-density polyethylene hybrid composites. *Journal of Applied Polymer Science* 141(29): e55683. https://doi.org/10.1002/APP.55683;REQUESTEDJOURNAL: JOURNAL: 10974628;PAGE:STRING:ARTICLE/ CHAPTER

Nasoudari, E., Ameri, M., Shams, M., Ghavami, V. & Bonyadi, Z. 2023. The biosorption of Alizarin Red S by Spirulina platensis; process modelling, optimisation, kinetic and isotherm studies. *International Journal of Environmental Analytical Chemistry* 103(3): 633–647. https://doi.org/10.1080/03067319.2020.1862814

Pratap, B., Kumar, S., Nand, S., Azad, I., Bharagava, R.N., Romanholo Ferreira, L.F. & Dutta, V. 2023. Wastewater generation and treatment by various eco-friendly technologies: Possible health hazards and further reuse for environmental safety. *Chemosphere* 313: 137547. https://doi.org/10.1016/J.CHEMOSPHERE.2022.137547

Qin, J., Dou, Y., Zhou, J., Candelario, V.M., Andersen, H.R., Hélix-Nielsen, C. & Zhang, W. 2023. Photocatalytic valorization of plastic waste over zinc oxide encapsulated in a metal-organic framework. *Advanced Functional Materials* 33(28): 2214839. https://doi.org/10.1002/ADFM.202214839;REQUESTEDJOURNAL:JOURNAL:16163028;WGROUP:STRING:PUBLICATION

Qin, K., Zhao, Q., Yu, H., Xia, X., Li, J., He, S., Wei, L. & An, T. 2021. A review of bismuth-based photocatalysts for antibiotic degradation: Insight into the photocatalytic degradation performance, pathways and relevant mechanisms. *Environmental Research* 199: 111360. https://doi.org/10.1016/J.ENVRES.2021.111360

Rabbani, M., Shokraiyan, J., Rahimi, R. & Amrollahi, R. 2021. Comparison of photocatalytic activity of ZnO, Ag-ZnO, Cu-ZnO, Ag, Cu-ZnO and TPPS/ZnO for the degradation of methylene blue under UV and visible light irradiation. *Water Science and Technology* 84(7): 1813–1825. https://doi.org/10.2166/wst.2021.360

Sedefoglu, N. 2024. Green synthesis of ZnO nanoparticles by *Myrtus communis* plant extract with investigation of effect of precursor, calcination temperature and study of photocatalytic performance. *Ceramics International* 50(6): 9884-9895. https://doi.org/10.1016/J.CERAMINT.2024.01.387

Ubaidullah, M., Al-Enizi, A.M., Shaikh, S., Ghanem, M.A. & Mane, R.S. 2020. Waste PET plastic derived ZnO@NMC nanocomposite via MOF-5 construction for hydrogen and oxygen evolution reactions. *Journal of King Saud University - Science* 32(4): 2397–2405. https://doi.org/10.1016/J.JKSUS.2020.03.025

Wan, W., Li, Y., Bai, S., Yang, X., Chi, M., Shi, Y., Liu, C. & Zhang, P. 2023. Three-dimensional porous ZnO-supported carbon fiber aerogel with synergistic effects of adsorption and photocatalysis for organics removal. *Sustainability* 15(17): 13088. https://doi.org/10.3390/SU151713088

Wang, Z., Fernández-Blanco, C., Chen, J., Veiga, M.C. & Kennes, C. 2024. Effect of electron acceptors on product selectivity and carbon flux in carbon chain elongation with *Megasphaera hexanoica. Science of The Total Environment* 912: 169509. https://doi.org/10.1016/J.SCITOTENV.2023.169509

Yoosefian, M., Ahmadzadeh, S., Aghasi, M. & Dolatabadi, M. 2017. Optimization of electrocoagulation process for efficient removal of ciprofloxacin antibiotic using iron electrode; kinetic and isotherm studies of adsorption. *Journal of Molecular Liquids* 225: 544–553. https://doi.org/10.1016/J.MOLLIQ.2016.11.093

*Corresponding author; email: ctnurulain@upm.edu.my